Submitted to The Astronomical Journal

HST/ACS Coronagraphic Imaging of the AU Microscopium Debris Disk

John E. Krist[1] et al.

ABSTRACT

We report on *HubbleSpaceTelescope* Advanced Camera for Surveys coronagraphic imaging of the recently-discovered edge-on debris disk around the nearby ($\sim$ 10 pc) M-type star AU Microscopium. The disk is seen in the V-band image from 0.″5 – 15" (5 – 150 AU). It has a narrow, concentrated midplane with a rather constant projected full-width-at-half-maximum of 2.5 – 3.5 AU within $r < 50$ AU that then increases to 6.5 – 9 AU at $r = 75$ AU. It has an approximately Lorenztian vertical brightness profile. The disk radial brightness profile is generally flat for $r < 15$ AU, then decreases gradually ($I \propto r^{-1.8}$) out to $r \approx 43$ AU, past which it falls rapidly ($I \propto r^{-4.7}$). The midplane is flat and aligned with the star at $r < 50$ AU and beyond that deviates by $\sim 3°$, resulting in a "bowed" appearance that was also seen in the ground-based discovery image. Three-dimensional modelling of the disk shows that the inner region ($r < 50$ AU) is seen at an inclination of $< 1°$ but the outer disk is inclined by $\sim 3°$. The inclination of the outer disk and the moderate forward scattering ($g \approx 0.4$) cause the apparent bowing. The intrinsic FWHM is 1 – 3 AU. The models indicate that the disk is clear of dust within $\sim$ 12 AU of the star, in general agreement with the previous prediction of 17 AU based on the infrared spectral energy distribution.

Subject headings: stars: circumstellar matter — stars: individual (AU Microscopium)

1. Introduction

A circumstellar debris disk represents the final stage of planetary system formation. Collisions of planetesimals (comets, asteroids, etc.) produce particles that are detected in

[1]Space Telescope Science Institute, 3700 San Martin Dr., Baltimore, MD 21218 (krist@stsci.edu)

thermal emission and scattered light. Without the continual replentishment of these grains, the disk would largely disappear due to radiation pressure, grain coagulation, and tidal interactions with planets, leaving behind a tenuous ghost of itself equivalent to the zodiacal cloud that surrounds our solar system. The lifetime of such disks is not fully understood, and it may depend strongly on the luminosity of the star. Highly luminous, early-type stars may blow away the disk within 10 – 20 Myrs. Later-type stars do not exert as much radiation pressure, so perhaps disks around them may have longer lives.

While numerous detections and images of optically-thick accretion disks have been made, only a few debris disks have been resolved. The current inventory of such disks was largely derived from *IRAS*-measured infrared excesses. This catalog is biased towards stars of spectral types A – F because their luminosities are high enough to heat a debris disk to the level that it could be detected by the satellite. More luminous stars would blow away such disks while cooler stars cannot heat them enough to be detected. Most of the debris disks that have been imaged so far are around A types (Beta Pictoris, Vega, Fomalhaut, HD 141569A, and HR 4796). Of these only the Beta Pic, HD 141569A, and HR 4796 disks have been seen in scattered light. Due to the sensitivity limits of *IRAS* a great uncertainty exists in the frequency and lifetime of debris disks around later-type stars. The disk around Epsilon Eridani, a K2V star and one of the greatest *IRAS* stellar excess sources, was detected by *IRAS* and imaged in emission (ref) because of its very close proximity (3.2 pc). The *SpitzerSpaceTelescope* should provide a good catalog of disk candidates around later-type stars.

Only two M-type stars not associated with molecular clouds have *IRAS*-measured infrared excesses: AU Microscopium and Hen 3-600 (Song et al. 2002). AU Mic is a M1Ve flare star and BY Dra-type variable ($V_{max} = 8.59, \Delta V \approx 0.15$; Cutispoto, Messina, & Rodonò 2003). Barrado y Navascués et al. (1999) identified AU Mic as part of the Beta Pictoris moving group, an association of nearby (10 – 50 pc) young stars. It is at a *Hipparcos*-measured distance of 9.9 pc and is about 10 Myrs old (Zuckerman et al. 2001). Its excess and distance implied that AU Mic had a substantial amount of circumstellar material, making it a good candidate for high contrast imaging. The *Hubble Space Telescope* (*HST*) Advanced Camera for Surveys (ACS) Science Team included AU Mic on its list of *HST* Cycle 12 targets as part of the team's circumstellar disk imaging program.

During Cycle 12 and preceeding the ACS observations, a disk was imaged around AU Mic in R-band using a coronagraph on a ground-based telescope (Kalas, Liu, & Matthews 2004; hereafter K04). Their image shows a disk that at first glance resembles that of Beta Pic. It is very close to edge-on and extends to a radius of at least 21" (210 AU). Their coronagraphic occulting spot prevented imaging within 5" of the star and the seeing prevented full resolution

of the disk midplane. The improved resolution of ACS and its ability to see closer to the star can provide more detailed views of this disk.

2. Observations, Photometry, and Processing

2.1. Observations

The *HST* observations of AU Mic (GJ 803) were made on 3 April 2004 with the ACS High Resolution Camera (HRC; 0.″25 pixel^{-1}, PSF FWHM=50 mas) as part of *HST* program 9987. The orientation of the telescope was specified to ensure that the disk was aligned along the detector diagonal. Two 0.1 second exposures were taken in F606W at a gain of 4 e$^-$ DN^{-1} to allow photometry of the star. After an automated acquisition exposure, five images (3×750s, 2×1400s) were obtained at a gain of 2 e$^-$ DN^{-1} with the star behind the small occulting spot (r=0.″9) that is located at the center of the HRC field. These exposures required a total of two orbits.

The ACS coronagraph suppresses the diffraction pattern of central star, reducing the surface brightness of its wings by a factor of ~ 7. The remaining flux from the occulted source is dominated by scattered light from the telescope optics for $r > 1.''5$ and by light diffracted by the occulting spot for $r < 1.''5$. The latter appears as concentric rings around the image of the spot. Because of the stability of *HST*, most of the residual light can be subtracted using an image of another star. HD 216149 was selected as the reference PSF because it is bright ($V = 5.4$) and is of similar color ($B - V$=1.47) to AU Mic. It is close enough to AU Mic in the sky to allow observation in an adjacent orbit, avoiding focus variations that could be caused by large attitude changes. As was done for AU Mic, two 0.1s exposures (gain = 4) were taken for photometry, though the star images were saturated by about 70 pixels, as expected (the shortest possible HRC exposure is 0.1s). After acquisition, 2 × 90s and 8 × 225s exposures (gain = 2) were taken with the star placed behind the small occulting spot. These exposures required a total of one orbit.

All of the images were calibrated by the *HST* pipeline. To account for vignetting around the occulting spot, the non-acquisition coronagraphic images were manually divided by the F606W spot flat available from the ACS reference files page at the STScI web site. The spot flat was first shifted to the appropriate position, as instructed on the web page, to account for the time-dependent spot position. The duplicate exposures were combined with cosmic ray rejection. Only the eight 225s exposures were used for creating the HD 216149 image. Note that at this stage, the images were not corrected for geometric distortion.

Photometry of the two stars is required to properly normalize the HD 216149 image prior

to subtraction from the AU Mic exposure. AU Mic was measured in the short, direct F606W image using a 0.″75 (30 pix) radius aperture. The HD 216149 short exposure was saturated, with column bleeding extending to 24 pixels above the star. Gilliland (2004) reported that when using the gain = 4 setting on the HRC, flux is conserved within saturated pixels so that an aperture that encompasses all of the saturated values should provide accurate photometry. The flux was therefore measured in the same-sized aperture as used for AU Mic. Both fluxes were then aperture and pixel-area-distortion corrected. The instrumental fluxes were converted to standard V magnitudes using the STSDAS SYNPHOT synthetic photometry program assuming M1V (for AU Mic) and M0III (for HD 216149) spectra. The resulting values are V=8.64±0.03 (AU Mic) and 5.46±0.05 (HD 216149). The AU Mic measurement is within the V brightness range reported by Cutispoto, Messina, & Rodonò (2003).

After renormalization, the HD 216149 coronagraphic image was iteratively shifted by subpixel amounts via cubic convolution interpolation and then subtracted from AU Mic until the residual scattered light pattern was minimized. This procedure appears to align the scattered light patterns of the two stars to within ±0.05 pix, aided by the high-spatial-frequency streaks in the residual pattern. After subtraction, the image was corrected for geometric distortion. The diffraction rings around the occulting spot were not as well subtracted. Their shapes and intensities are quite sensitive to the alignment of the star behind the spot, which was different by 13 mas between the two observations. They are also sensitive to focus changes and small differences between the spectra of the stars over the filter's bandpass. Their residuals, which appear as alternating positive and negative rings, are the dominant source of error for $r < 1.''5$, where they create localized uncertainties of ±30% on 0.″1 scales in the disk brightness. Beyond this region, the background is dominated by scatter-subtraction residuals, which cause pixel-to-pixel errors of < 10%. The residual level indicates that the using the coronagraph with PSF subtraction improved the disk-to-background contrast by ∼ 150× compared to direct imaging without subtraction.

3. Results

The AU Mic disk stands out against the background PSF structure in the ACS coronagraphic image (Figure 1) even before PSF subtraction. The northwestern side is detected out to the edge of the detector, 15.″25 (∼150 AU) from the star, and the southeastern side to ∼14" (∼140 AU). The disk can be seen to a height of 2.″5 (25 AU) above the midplane. The observed radial and height extents in the image are sensitivity-limited. The interior of the occulting spot is filled with light that was not blocked by the spot (which is located in

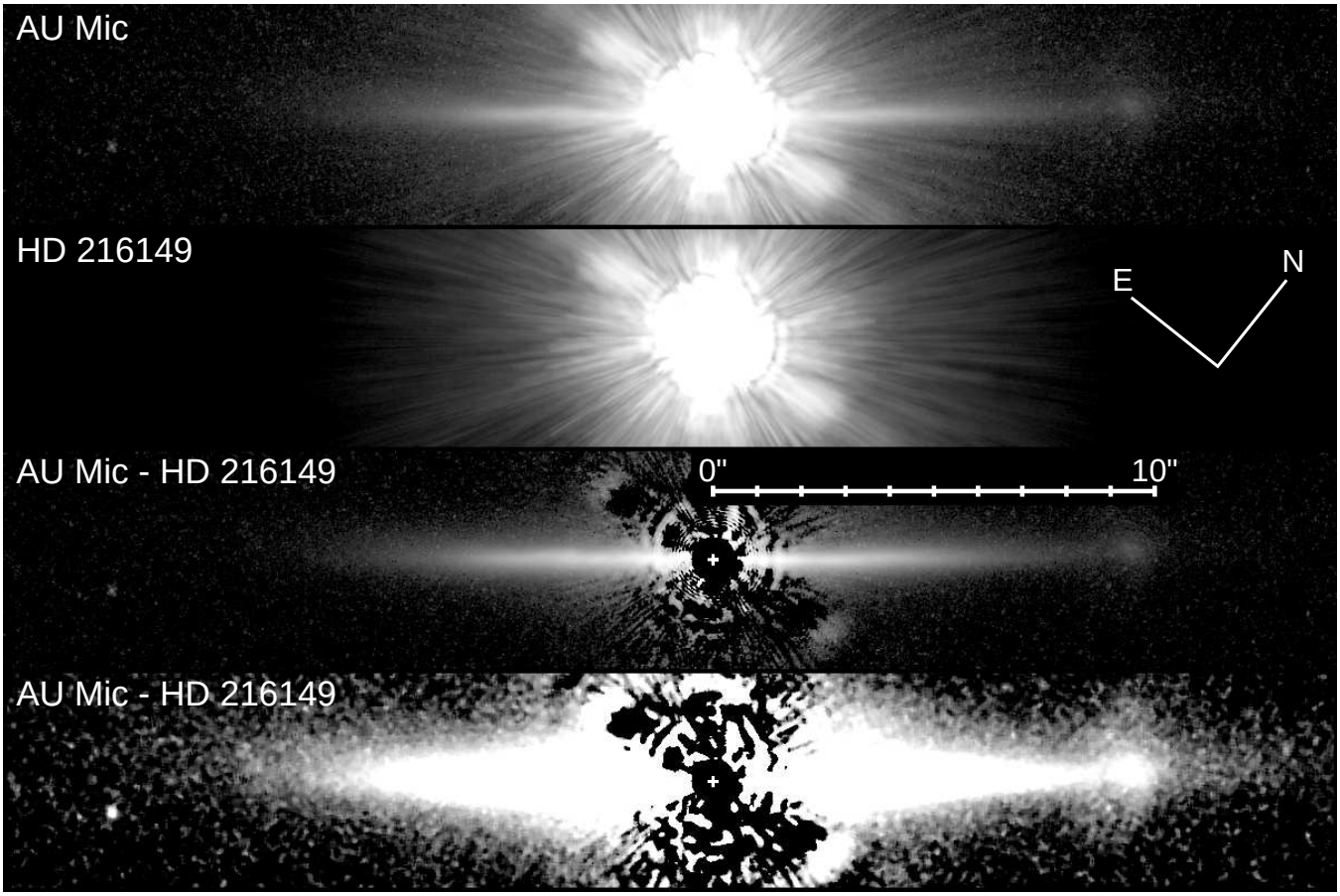

Fig. 1.— ACS F606W (wide-V) coronagraphic images of AU Mic and the reference PSF star HD 216149, all displayed with logarithmic intensity scaling. The bottom image is smoothed and shown using a stronger stretch to reveal fainter features.

the aberrated *HST* beam) and was afterwards modified by the corrective ACS optics. An image of the star at the spot's center allows accurate measurement of the stellar position. An extended source can be seen superposed on the NW midplane, 9.″6 from the star.

The PSF-subtracted image more clearly reveals the disk with most of the diffracted and scattered light from the star removed. Because the disk is fairly bright close to the star and the corrective optics modify the aberrated light that passed by the occulter, the disk can actually be seen inside the spot, to within 0.″75 (8 AU) of the star.

The extended source detection limit in the subtracted image was determined by adding 1" wide, uniform-intensity squares to the data at 3" and 9" from the star, perpendicular to the circumstellar disk. Their intensities were adjusted until they could no longer be detected for $V > 23.2 \pm 0.2$ (3") and $V > 23.8 \pm 0.1$ (9") mag arcsec^{-2}.

3.1. Disk Morphology

To allow accurate measurement of the disk orientation, simple spatial filtering was applied to highlight the midplane. The image was subtracted by a copy of itself that was smoothed by a 3 × 3 pixel median filter. This removed the extended vertical wings while preserving the sharp peak of the midplane seen within 5" of the star (Figure 2). A line fit to the resulting image shows that the inner ($r < 5$") midplane is oriented at PA=128.6° ± 0.2°. There are small ($\sim 0.''25$), oscillations in the midplane position about this line, which passes directly through the star. Superposing this line over the original image highlights the deviation of the outer ($r > 5$") midplane from the inner (Figure 3). At large angles, the disk looks "bowed", an effect noted by K04 and also seen in the Beta Pic disk (Kalas & Jewitt 1995). The apparent outer disk midplane measured by-eye at r=12.″5 is oriented along PA=311.1° ± 0.7° on the NW side and PA=125.6° ± 0.7° on the SE. These angles are

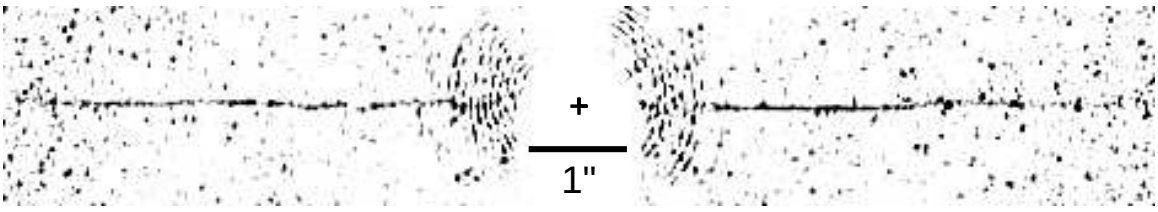

Fig. 2.— ACS coronagraphic PSF-subtracted image of AU Mic after subtraction of a median-smoothed copy of itself, highlighting the higher spatial frequency structures, notably the flat, sharp disk midplane (other features are noise and PSF subtraction residuals). Inverse intensity and the same orientation as Figure 1.

consistent with those reported in K04.

Radial surface brightness profiles along the disk midplane (including provision for the "bow") are shown in Figure 4. Both sides of the disk appear to have very similar profiles, though the NW side is brighter beyond 10" (100 AU) by $\sim 2\times$ relative to the SE. There are $\sim 20\%$ dips at $r = 2\farcs3$ (23 AU) on both sides that appear to be genuine and not PSF subtraction artifacts. Between $4\farcs3$ and $5\farcs3$ the SE side is $\sim 25\%$ brighter than the NE. Within $1\farcs5$ the subtraction residuals are too great to identify any localized asymmetries of less than 30%.

The mean midplane radial brightness profile may be reasonably divided into three zones described by different power laws. The inner zone ($r < 1\farcs5$) is nearly flat ($I \propto r^{-0.3}$). The middle zone ($1\farcs5 < r < 4\farcs3$) has a moderate radial decrease in brightness ($I \propto r^{-1.8}$) and the outer ($r > 4\farcs3$) drops off rapidly ($I \propto r^{-4.7}$). The latter indicates a more rapid dropoff than the $\sim r^{-3.8}$ measured by K04 between 6" – 16". This is likely due to their use of a $1\farcs2$ wide measurement aperture on an image that did not fully sample the disk perpendiculary to the midplane, which the *HST* image does.

The inner disk's vertical brightness profile (Figure 5) shows a sharp midplane with extended wings. It can be reasonably well characterized for disk radii <5" by a Lorentzian profile: $I(z) = 1/(1 + z^2/h^2)$, where $2h$ is the profile full-width-at-half-maximum (FWHM) and z the height above the midplane. Note that we find this particular shape to be a convenient description of the disk profile and that we do not assume any physical meaning to it. The profiles are generally symmetric about the midplane for $r < 5''$ but beyond this the disk is brighter on the NE side of the midplane. The outer disk profile is more rounded and lacks a prominent midplane.

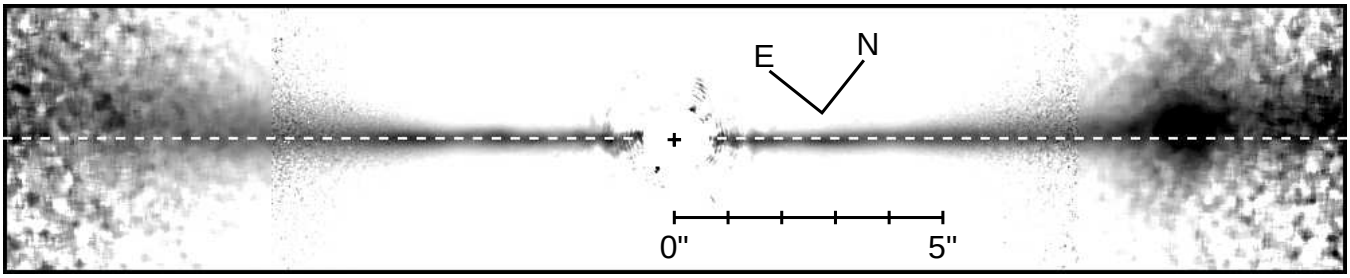

Fig. 3.— ACS image of the AU Mic disk normalized by the radial brightness profile power laws described in the paper and displayed in inverse intensity. Data beyond $7\farcs5$ has been median-smoothed. The "bowing" can be seen in the outer disk as an upwards deviation from the horizontal line defined by the inner midplane.

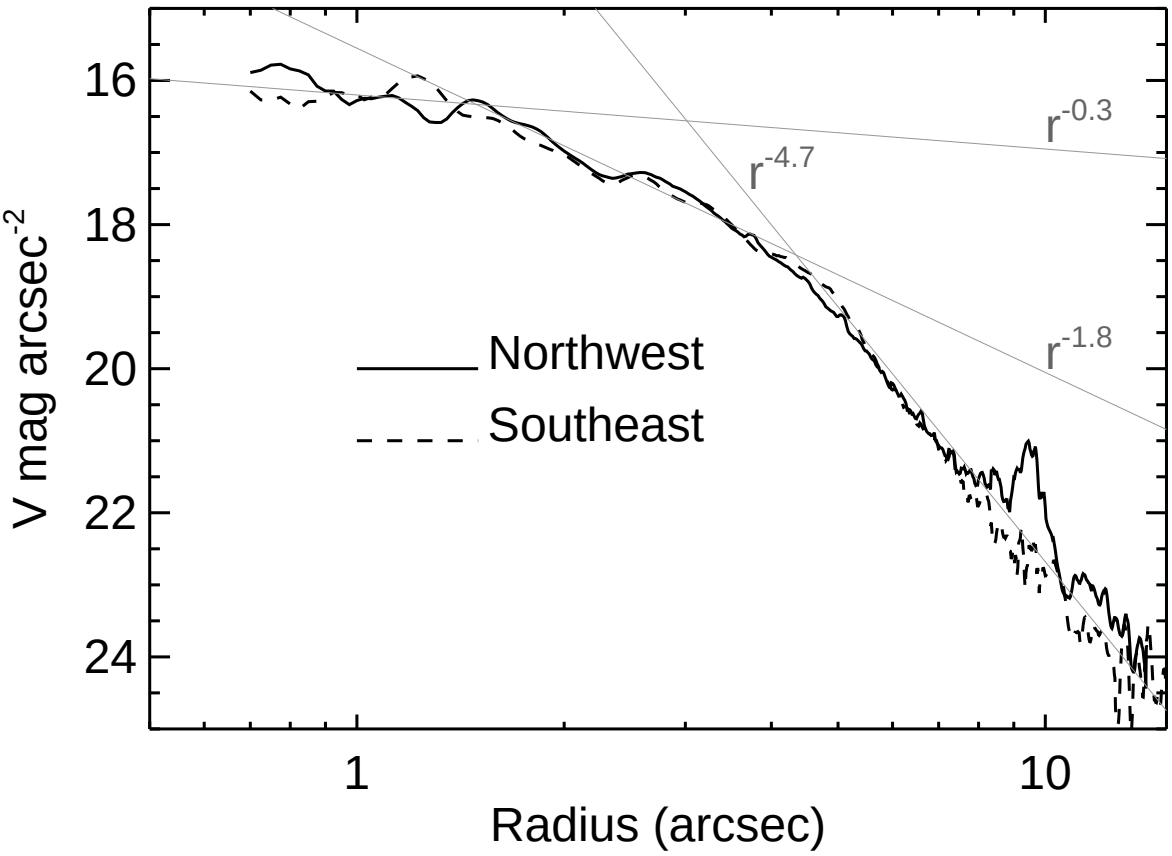

Fig. 4.— Radial surface brightness profiles following the AU Mic disk midplane (including the bow) measured over 0.″25 × 0.″25 pixels. Power law profiles are overplotted.

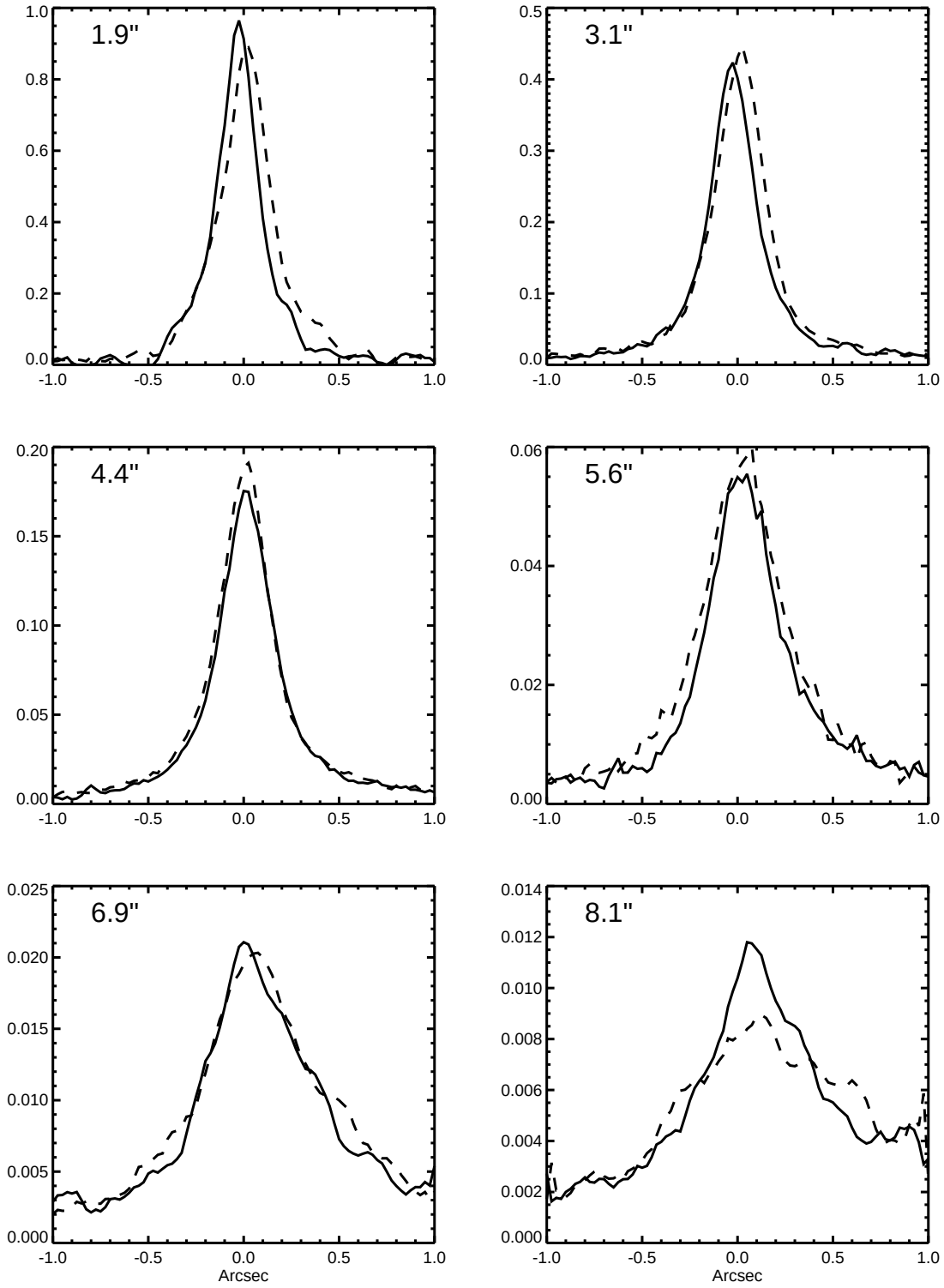

Fig. 5.— AU Mic disk intensity cross-sections perpendicular to the midplane at various radii. The solid lines are the NW disk, dashed SE. The NE side of the disk is towards the right.

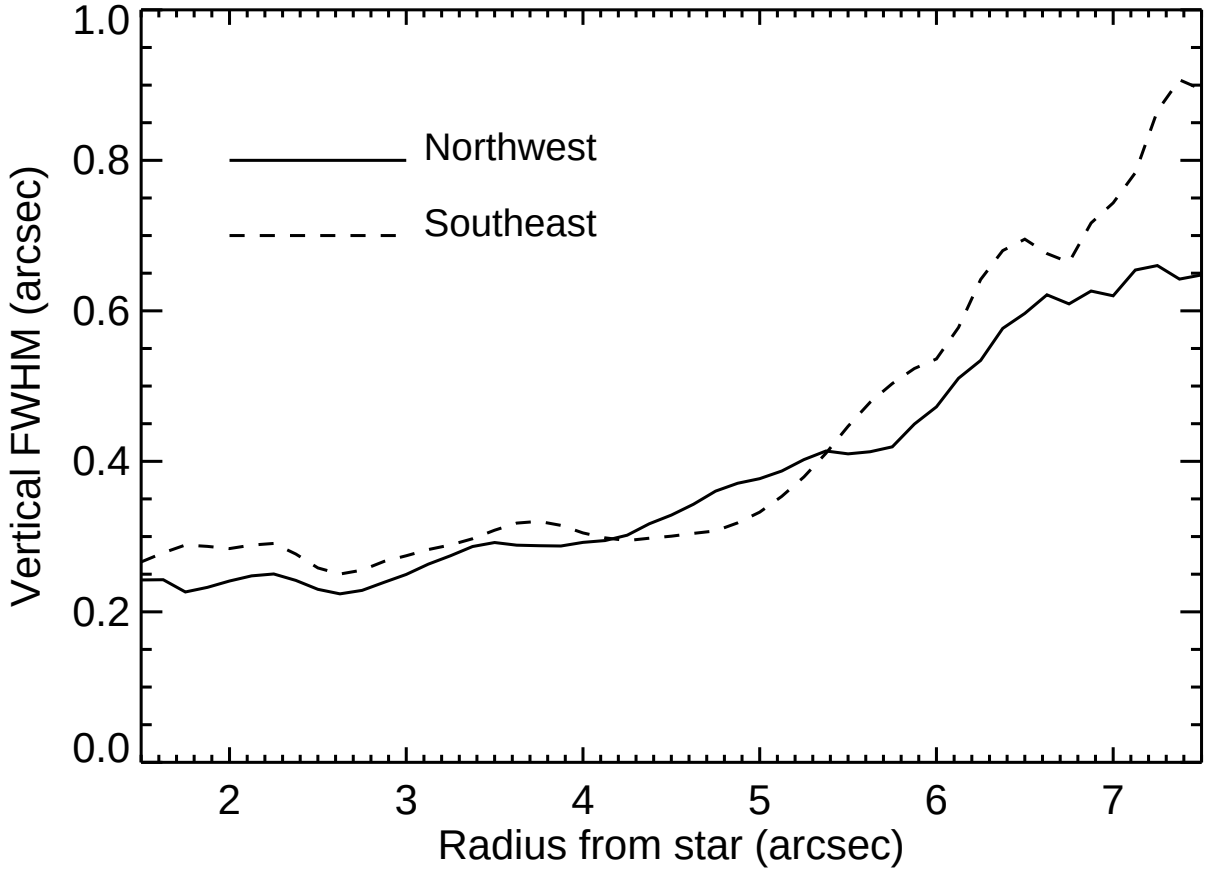

Fig. 6.— Measured AU Mic disk full-widths-at-half-maximum.

The FWHM at each radius was measured by fitting a Lorentzian profile to a vertical cross-section of the image after the image was smoothed by 5 pixels along the direction of the midplane. As shown in Figure 6, the inner disk is rather flat, but the outer part begins to flare beyond 5". The FWHM for $r < 5''$ (50 AU) is $0\farcs25 - 0\farcs35$ (2.5 – 3.5 AU). At $r = 7\farcs5$ (75 AU) the FWHM on the SE side is $0\farcs9$ (9 AU) and $0\farcs65$ (6.5 AU) on the NW. The change in FWHM along the SE side can be approximately described by two power laws: $FWHM \propto r^{0.07}$ for $1\farcs5 < r < 4\farcs6$ and $r^{2.4}$ for $4\farcs6 < r < 7\farcs5$. The equivalent relations for the NW side are $FWHM \propto r^{0.07}$ for $1\farcs5$ – $3\farcs0$ and $r^{1.0}$ for $3\farcs0$ – $7\farcs5$.

3.2. Disk Modelling

Derivation of the physical distribution and properties of the dust in the disk directly from the image is prohibited by the integrated effects of forward scattering and radial density variations seen along the line of sight. They can be estimated from three-dimensional scattering models optimized to match the observed image. We have explored the range of parameters by fitting model images to the F606W data.

The modeling code computes the integrated, singly-scattered reflected light in the disk along the line of sight. Because the AU Mic disk is optically thin (K04), it should be possible to adequately explore parameter space using models that show only singly-scattered photons. The fraction of multiply-scattered photons in the image should be insignificant. Assuming axial symmetry, the reflecting surface density $\rho(r, z)$ at radius r and height z is characterized by $\rho(r, z) = \rho_0(r/r_0)^{\alpha}\phi(z, h)$ where ρ_0 is the midplane density at some fiducial radius r_0 and the scale height of the vertical distribution profile $\phi(z)$ varies as $h = h_0(r/r_0)^{\beta}$. An albedo of 0.5 is assumed. We examined two vertical distributions that could produce sharp midplanes with extended wings: an exponential power law where $\phi(z) = |z/h|^{\delta}$, and a Lorentzian profile where $\phi(z) = 1/(1 + (z/h)^2)$. While capable of doing so, no models were generated using a Gaussian profile, which poorly matches the observed shape. The code can compute a model with contiguous annular zones, each with independent α, β, inclination, midplane position angle, and outer radius (the outer radius of one zone defines the inner radius of the next). The midplane densities and scale heights are constrained to be continuous across the zone interfaces. The inner radius of the innermost zone also defined.

The intensity of reflected light from each point in the three-dimensional model is modified by an angle-dependent scattering phase function. Three options are available: a Henyey-Greenstein (H-G) phase function with a variable asymmetry factor (g), the zodiacal phase function of Hong (1985) which is a summation of three H-G functions, and a cometary phase function (Artymowicz 1997).

An iterative, non-linear least squares fitting routine was used to optimize the disk parameters by generating models and comparing them to the image. Both sides of the disk were simultaneously fit using the model, which is axisymmetric about the star within each disk zone. To avoid the brighter inner regions from completely driving the results, the weights for all of the pixels at each radius were muliplied by the inverse of the peak midplane intensity at that radius. Regions covered by the midplane extended source at $r = 9\farcs6$ and within $0\farcs75$ of the star were given zero weight. The model was convolved with a Tiny Tim PSF model (Krist & Hook 2004). During the comparisions pixels at $r > 7\farcs5$ in both the data and model were smoothed using a 7×7 pixel median filter to reduce the pixel-to-pixel noise in those faint regions of the image (the apparent disk midplane is sufficiently extended at those radii to be unaffected by this smoothing). All of these models were computed with a 250 AU outer radius and 40 AU maximum height (the vertical density falloff is sufficiently rapid that the assumed height is not a significant parameter).

Initial fits were made using the available scattering phase functions, exponential and Lorentzian vertical profile shapes, and different starting parameters. These initial models had three zones corresponding to those used to characterize the radial brightness profile, with the outer radii of the two inner zones allowed to vary and an inner radius of 3 AU (which is relatively unimportant since the disk cannot be seen to within $\sim$ 7 AU). The position angles and inclinations of the zones were constrained to be the same. There is a general set of results from these fits. The inclinations were all $< 1°$. H-G scattering phase functions were favored, with $g < 0.5$ (moderate forward scattering, as $g = 0$ implies no phase dependence). Those fits that used the zodiacal or cometary phase functions were unable to produce reasonable matches for $r > 20$ AU without making the inner region several times too bright (even given the large subtraction residual errors there). All of the fits had extremely large values for a ($\gg 10000$) in the inner annular zone, implying that it is essentially clear of reflecting material. The disk is fairly flat ($|\beta| < 0.5$) except in the outer zone. Fits using a power law vertical profile favored a sharper-than-exponential shape, with $\delta = 0.88 - 0.95$ and scale heights of $h \approx 1$ AU in the inner disk. Lorentzian profiles were slightly favored over the exponentials with vertical FWHMs of ~ 1.8 AU. The low inclination appeared to be mostly constrained by the inner disk as it was not sufficient to cause the bowing and reduction in the midplane sharpness seen in the outer disk. These early fits were useful in revealing the small-scale asymmetries in the disk (Figure 7).

Based on these initial results, a more complex model was applied. The inner zone was deleted and the inner disk radius (inside of which the density instantly drops to zero) was set to an initial value of 10 AU and allowed to vary. The remaining two outer zones were divided into four based on the residuals seen in the initial fits, providing greater freedom to fit smaller variations in the disk. The zones' outer radii varied except for the last one which

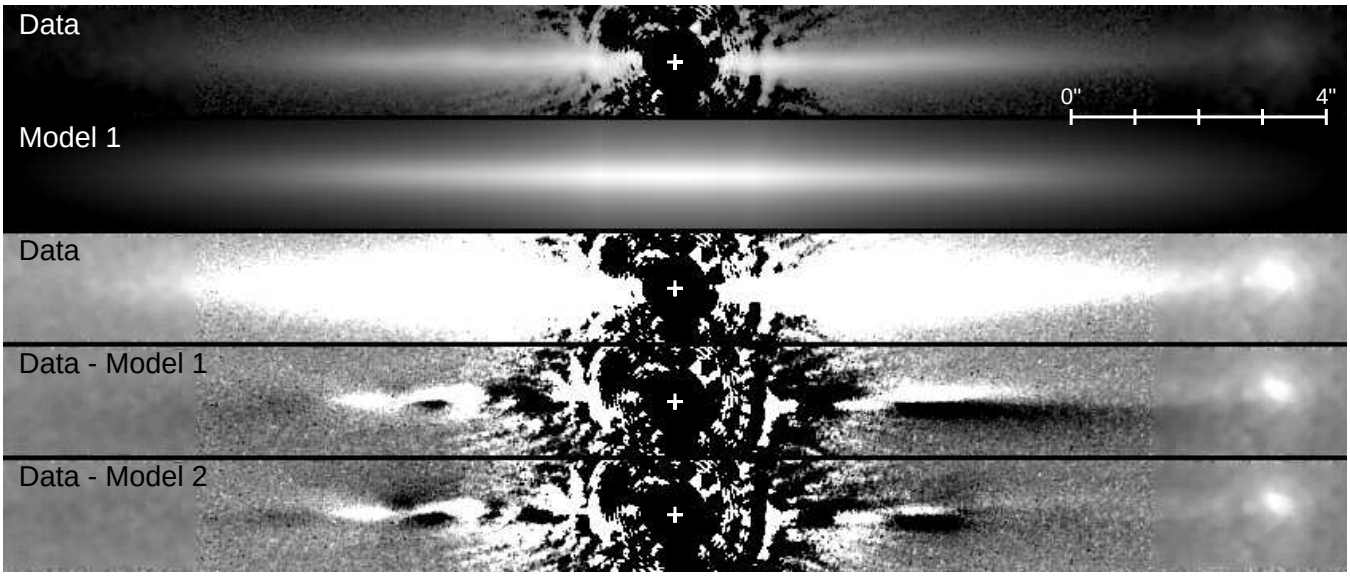

Fig. 7.— Comparisons of the AU Mic disk image with three-dimensional scattering models. The top two images show the observed data and the simple, three-zone model (Model 1) displayed with the same logarithmic intensity stretch. Below them is the observed image and the Data - Model difference images displayed with the same strong linear stretch. Model 2 is the more complex model in which each zone may have different inclinations. The cross marks the position of the star.

was fixed at 250 AU. The inclination and position angles of each zone were also allowed to vary. A Lorentzian profile was used as it provided the best results in prior runs. A number of fits were run with different initial parameters to investigate the robustness of the results. These fits successfully reproduced all of the major features of the disk (Figures 7 – 9).

In the final fit, the inclination within ∼83 AU is almost exactly edge-on ($|\theta| \leq 1°$) while the outer disk is more inclined ($\theta \approx 3.5°$) with the NE pole tilted towards us. The combined effect of forward scattering ($g \approx 0.4$) and the inclination of the outer disk explain the bowing (and the sign of the inclination its direction), while the near-zero inclination of the inner disk explains the straight midplane at smaller radii.

The intrinsic disk thickness, as described by the h_0 and β values, decreases with radius within the first zone from $FWHM \approx 1.5$ AU at the inner wall ($r \approx 12$ AU) to ∼0.4 AU at $r \approx 25$ AU. It then increases almost linearly with radius, so that at $r = 75$ AU the FWHM is ~ 2 AU. The radial decrease within the first zone may not be real but rather could be a result of the local asymmetries driving the fits to nonphysical solutions. The trend in the outer zones is more believable as the local asymmetries there are weaker. Out to $r \approx 90$ AU the intrinsic disk thickness is less than the projected thickness measured directly from the image (past this radius the measured FWHM values are not accurate due to the low surface brightness of the disk and its deviation from a Lorentzian vertical profile). At 50 AU, the projected thickness is 2× the intrinsic. This indicates that much of the apparent increase in thickness with radius is not physical but is a projection effect caused by the inclination of the outer disk. The inclination also causes the intrinsically sharp midplane to appear rounder at larger radii, thereby negating the need for a different vertical profile shape in the outer disk.

The midplane density increases by $\sim$ 50% within the inner zone (12 – 25 AU) and decreases by about the same within the next (25 – 45 AU), after which it falls as $\sim r^{-3.5}$. This may indicate that at a finer scale there is a smooth turnover in the density profile over 12 – 45 AU. The positive α within the inner zone may be suspect for the same reason as its negative β. If all of the zones were coplanar, then the midplane extinction based on the radial density profiles would be < 0.1 mag, confirming that the disk is optically thin.

There is likely some tradeoff between the variation in brightness with radius due to the scattering phase function and from the radial density falloff as characterized by a. A tighter constraint on the phase function would be possible if the disk could be seen closer to the star than is allowed with the occulting spot. The multizonal nature of the disk has been somewhat artificially decomposed into a set of separate power law descriptions that only provide constraints on the continuity of the density variation within a zone, without a rigorous physical basis for them. Given the number of free parameters and the very limited

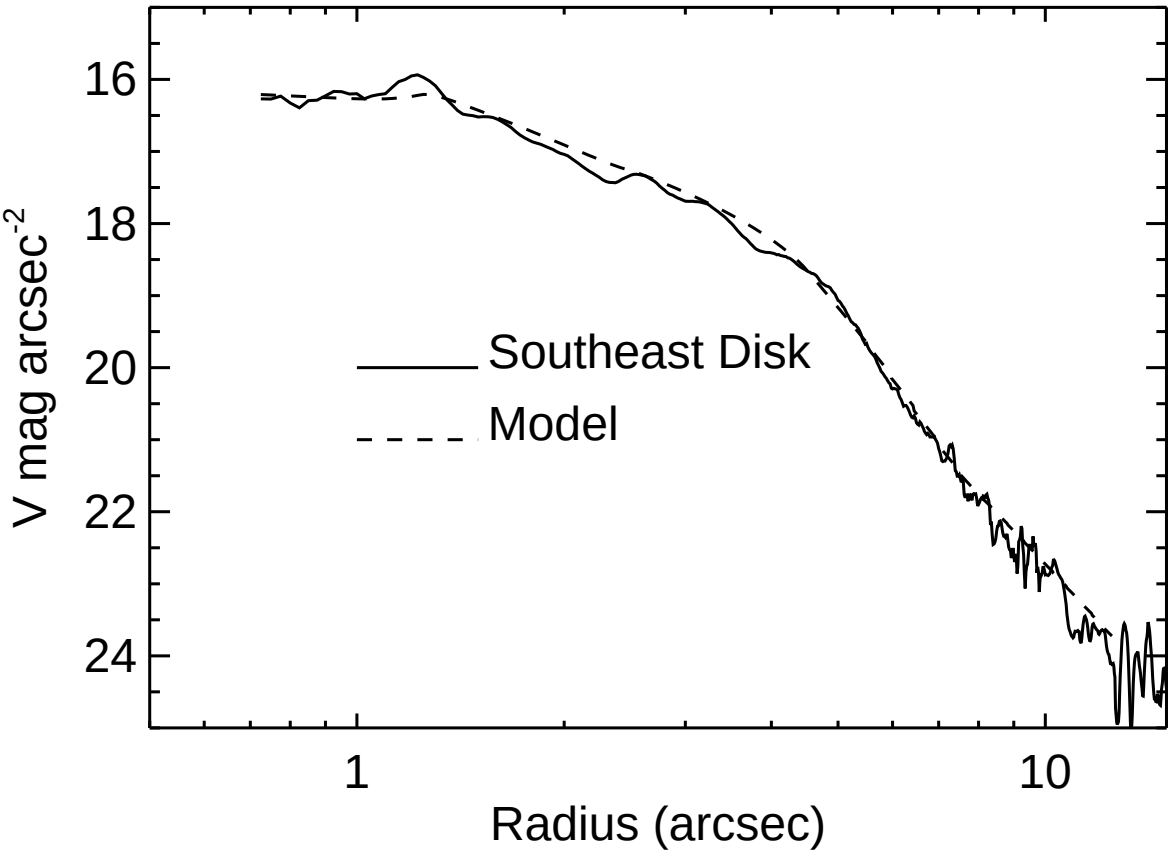

Fig. 8.— Comparison of the radial surface brightness profiles of the SE side of the disk and the equivalent section of the final model.

number of constraints, it is not possible to derive very robust values for both g and α in the case of a multizonal, edge-on disk. This would not be a problem if the disk could be resolved in thermal emission, where phase effects are not present, but that is a job that must wait for future observatories like ALMA.

3.3. Extended Source in the Midplane

The resolved, centrally-concentrated source seen along the NW disk midplane at 9.″6 from the star appears to be a nearly face-on spiral galaxy (Figure 10). A smoothed image subtracted by the disk model reveals what appear to be spiral arms extending 1.″7 from the nucleus. This object was also seen as an extended, featureless source in the K04 R-band image. There was insufficient proper motion of the star between the the time of our observation and that of K04 ($\sim$ 6 months) to confirm that it is not co-moving with AU Mic.

4. Discussion

The $r < 12$ AU clearing implied by the model fits is consistent with $r < 17$ AU one derived by Liu et al. (2004) from the AU Mic infrared spectral energy distribution. Given the low luminosity of the star it cannot be caused by dust sublimation or zonal segregation of the grains by radiation pressure (Takeuchi & Artymowicz 2001). As Liu et al. suggest, tidal interaction of the dust with an unseen, low-mass companion within the clear zone is a strong possibility. They report no detection of an infrared companion during a "shallow" search using adaptive optics on Keck, so deeper imaging is certainly warranted. Given the nearly exact edge-on orientation of the disk, AU Mic is a good candidate for detecting potential planetary transits.

A low-mass perturber may explain the asymmetries seen in the disk and may also cause the inclination difference between the inner and outer disk. This appears equivalent to the warping seen in the Beta Pic disk, which has been explained using hypothetical companions (refs). While the tilt of the pole of the Beta Pic inner disk is mostly in the plane of the sky, in AU Mic it appears inclined mainly along the line of sight.

The AU Mic disk seems quite thin, with an intrinsic FWHM derived from the model fits of $\sim$ 1 AU for $r < 50$ AU increasing to $\sim$ 3 AU by $r = 100$ AU. Note that these widths are different than those measured directly from the image (2 – 3 AU) due to the integrated projection and inclination of the disk along the line of sight. For comparison, the Beta Pic disk has a projected FWHM of 15 – 18 AU between $r = 20 - 120$ AU, and its intrinsic

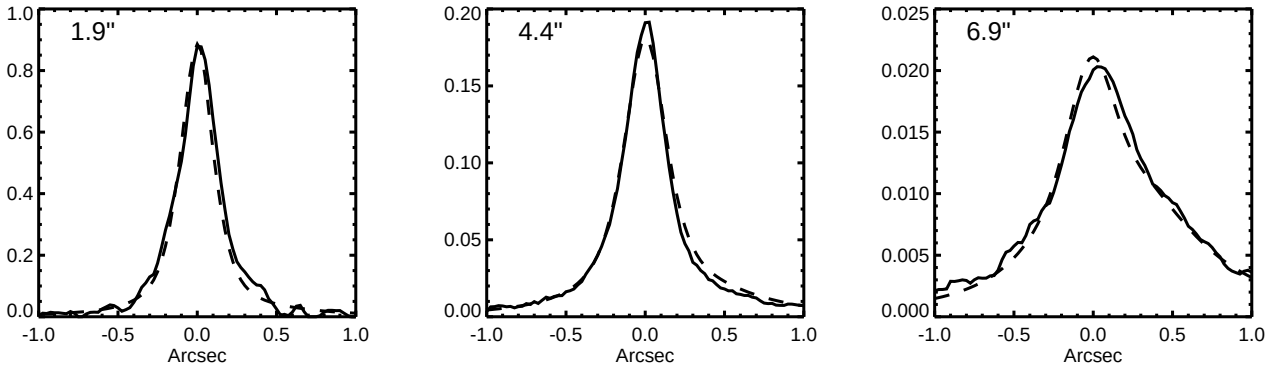

Fig. 9.— AU Mic disk observed and model intensity cross-sections perpendicular to the midplane at various radii. The solid lines are the SE disk, dashed are from the model. The NE side of the disk is towards the right.

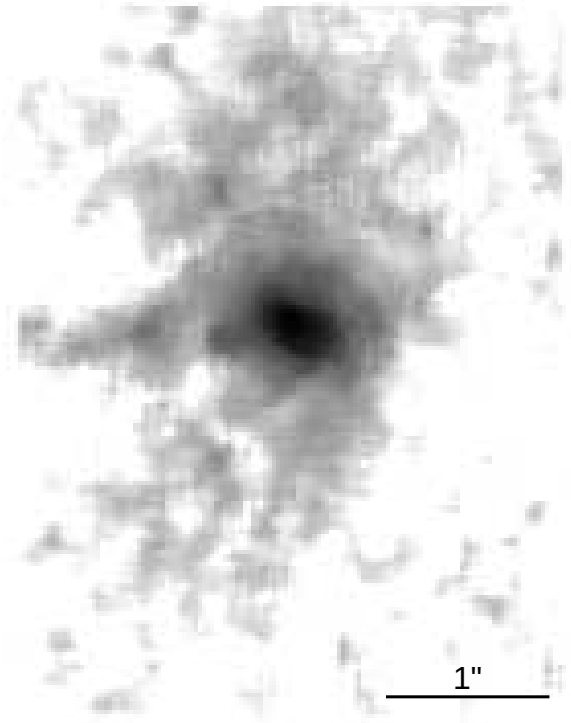

Fig. 10.— Extended feature, presumeably a galaxy, that lies along the NW side of the disk. It is shown here in reverse intensity with the final disk model subtracted and after smoothing. Same orientation as Figure 1.

thickness at $r = 100$ AU as derived from modelling by Kalas & Jewitt (1995) is $FWHM = 7 - 14$ AU. The approximately-Lorentzian vertical profile of the AU Mic disk is very similar to that of Beta Pic's for $r < 115$ AU as measured in recent ACS coronagraphic images. The Beta Pic profile actually becomes sharper than Lorentzian past 115 AU.

We stress again that the application of a Lorentzian profile simply provides a reasonable description of the vertical density distribution, which may be intrinsically more complex (e.g. the sum of multiple Gaussian distributions of various scale heights). It is possible that the AU Mic disk has a sharper profile and is more inclined than the fits indicate. However, the fits using variable-power exponential profiles that could produce sharper profiles had inclinations similar to those using Lorentzian profiles. There are certainly some parameter degeneracies that can create trade-offs between the assumed vertical profile, inclination, and scale height.

Forward scattering places some contraints on the inclination as greater tilt would cause the disk on one side of the midplane to become significantly brighter than on the other. The scattering phase parameter value of $g \approx 0.4$ implies that the grain population is different from those found in optically-thick disks around younger stars such as HH 30 (Burrows et al. 1996) or the ISM, where $g \approx 0.65$. It does lie within the $g = 0.3 - 0.5$ range derived for Beta Pic by Kalas & Jewitt (1995) and is slightly more than the $g = 0.25 - 0.35$ of HD 141569A (Clampin et al. 2003). The brightness profile of the inner region of the disk, especially within 1" – 2" of the star, places the greatest constraint on the choice of the scattering phase function. Despite the large subtraction errors within $r < 1\farcs5$, it is clear that the zodiacal and cometary phase functions are inappropriate, as they have too much forward scattering (at least $2\times - 4\times$ more than H-G at scattering angles 10° from the line-of-sight). There are probably some small degeneracies between the scattering phase function and the power-law profiles used to describe the radial density distribution.

The properties of the AU Mic disk grains are of particular interest because this is the first debris disk to be seen in scattered light that is not affected by significant radiation pressure. The small (< 1 μm) particles produced in planetoid collisions are not immediately blown away as they would be in a disk around a higher luminosity star. The grain population may be quite different than those in other imaged debris disks such as Beta Pic. The disk appears to have little gas (Liu et al. 2004), so there is also not much drag except for Poynting-Robertson and (in the inner disk) tidal effects. Thus, there may be a relative surplus of small grains, which should cause the disk to appear blue relative to the star. In comparison, the Beta Pic disk has an essentially neutral color and HD 141569A is red. At the moment the only hint of the dust characteristics is forward scattering, which indicates the presence of submicron particles. The ACS Science Team currently plans to obtain multicolor images of

the disk with *HST* within the next year that should better constrain the grain properties.

5. Conclusions

The disk of AU Mic has been imaged in scattered light at high resolution with *HST* in the V passband to within $\sim 0\farcs5$ (5 AU) of the star. The surface brightness profiles of the two sides of the disk are remarkably similar, especially when compared to those of the Beta Pictoris disk. Only slight, localized brightness asymmetries are seen, except at $r > 100$ AU where the NW is $\sim 2\times$ brighter than the SE. An extended feature at $r = 96$ AU on the NW midplane appears to be a galaxy.

Modelling indicates that the inner ($r < 50$ AU) region is seen very close to edge-on ($\theta < 1°$) while the outer is inclined $\sim 3°$ towards us. The disk appears to be clear of material within 12 AU of the star, consistent with the infrared SED. The disk has a fairly sharp midplane with an intrinsic vertical FWHM of < 1 AU at $r < 50$ AU which increases to ~ 3 AU at $r = 100$ AU. The forward scattering is comparable to that seen in other debris disks, namely Beta Pic and HD 141569A.

6. Acknowledgements

The ACS instrument was developed under NASA contract NAS5-32864, and this research was supported by NASA grant NAG5-7697.

REFERENCES

Artymowicz, P. 1997, in Annui. Rev. Earth Planet Sci., ed. R. Jeanloz, A. Albee, & K. Burke (Palo Alto: Annual Reviews, Inc.), 175

Barrado y Navascués, D., Stauffer, J. R., Song, I., & Caillault, J.-P. 1999, ApJ, 520, L123

Burrows, C. J., et al. 1996, ApJ, 473, 437

Clampin, M., et al. 2003, AJ, 126, 385

Cutispoto, G., Messina, S., & Rodonò, M. 2003, A&A, 400, 659

Gilliland, R. L. 2004, ACS Instrument Science Report ISR 04-01 (Space Telescope Science Institute)

Hong, S. S. 1985, A&A, 146, 67

Kalas, P. & Jewitt, D. 1995, AJ, 110, 794

Kalas, P., Liu, M. C., & Matthews, B. C. 2004, Science, 303, 1990

Krist, J. E. & Hook, R. 2004, Tiny Tim Users Manual v6.2 (www.stsci.edu/software/tinytim)

Liu, M. C., Matthews, B. C., Williams, J. P., & Kalas, P. G. 2004, ApJ, in press

Song, I., Weinberger, A. J., Becklin, E. E., Zuckerman, B., & Chen, C. 2002, AJ, 124, 514

Takeuchi, T. & Artymowicz, P. 2001, ApJ, 557, 990

Zuckerman, B., Song, I., Bessell, M. S., & Webb, R. A. 2001, ApJ, 562, L87